

High-Quality Pulse Compression Using a Hybrid All-Bulk Multipass Cell Scheme

V. W. Segundo Staels^{1,*}, E. Conejero Jarque^{1,2}, and J. San Roman^{1,2}

¹Grupo de Investigación en Aplicaciones del Láser y Fotónica, Departamento de Física Aplicada, Universidad de Salamanca, E-37008 Salamanca, Spain

²Unidad de Excelencia en Luz y Materia Estructuradas (LUMES), Universidad de Salamanca, Salamanca 37008, Spain

*vwsstaels@usal.es

January 23, 2025

Abstract We present a detailed numerical study of ultrashort pulse compression using a three-stage hybrid all-bulk multipass cell scheme. By operating in the enhanced frequency chirp regime, we achieve the compression of pulses from around 180 fs to 4 fs pulse duration (a total compression factor above 45), with side lobes contributing with intensity values lower than 0.2 % of the peak intensity. Optimal conditions for the enhanced frequency chirp regime propagation have been identified, enabling smooth spectral broadening and high-quality temporal profiles. The first two stages are based on bulk multipass cells to achieve a controlled spectral broadening, while the third stage consists of a thin plate to reach the spectral broadening needed for few cycle pulses without leaving the enhanced frequency chirp regime.

1 Introduction

Ultrashort, high-intensity laser pulses have revolutionized various scientific and industrial fields, driving relevant advances in areas such as strong-field physics, attosecond science, multiphoton microscopy, and materials science [1–3]. These applications often demand pulses with durations of a few tens of femtoseconds or even shorter, enabling the investigation of ultrafast processes with unprecedented temporal resolution. To overcome the bandwidth limitations of conventional lasers and achieve the desired shorter pulse durations, various post-compression techniques have been developed. Most of these techniques rely on the principle of spectrally broadening the laser pulse through the introduction of a nonlinear phase modulation and then compensating the acquired spectral phase using an external compression device, such as a diffraction grating or chirped mirrors [4, 5].

Among the various post-compression methods, nonlinear propagation in multipass cells (MPCs) have emerged as a promising technique, positioning at the forefront of these methods for high average power laser systems [6–8]. MPCs are based on the propagation of a laser pulse through a nonlinear medium contained in a resonant optical cavity, such as a Herriott cell [9]. The cavity is designed so that the pulse makes multiple passes through the medium, accumulating a significant nonlinear phase shift through self-phase modulation (SPM).

Advantages of MPCs include high transmission efficiency, excellent beam quality, scalability to high power, and flexibility in the choice of nonlinear medium. It has also been verified that it is possible to achieve self-compression of laser pulses in setups based on multi-pass cells [10–12]. In particular, gas-filled MPCs offer smooth nonlinear response, broad transparency range, and reduced thermal effects, but are limited by their lower nonlinearity and more complex setup. Multipass cells including bulk media, on the other hand, show higher nonlinear responses and simpler setups. While they may present challenges such as thermal effects and spectral bandwidth limitations, recent work has demonstrated that bulk MPCs can achieve efficient few-cycle pulse compression with remarkable stability and spectral broadening, showing their potential as a compact and effective post-compression scheme [13]. Another key benefit of bulk MPCs, compared to propagation through thin plates alone, is their ability to better preserve the spatio-spectral homogeneity of the pulse [14].

A possible problem when shortening pulses with large compression factors is the loss of temporal quality [15]. Improving the pulse temporal quality in MPC post-compression can be achieved using various advanced techniques, such as employing higher-order dispersion management or dividing the compression into multiple stages [15], or via the nonlinear elliptical polarization rotation [16–19]. A different approach is to exploit the enhanced frequency chirp regime (EFCR), which involves working in a region of parameters in which the SPM and the group velocity dispersion are both relevant effects, generating smooth spectra and, therefore, helping to enhance the temporal quality of the compressed pulse.

Although the EFCR was first reported in the 1980s in the context of optical fibers [20, 21], it has been recently extended to gas-filled MPCs. Theoretical studies [22, 23] and experimental

demonstrations [24] have confirmed the effectiveness of EFCR in MPCs to achieve short pulses with improved temporal quality and increased peak pulse power by using dispersive mirrors or tuning the gas pressure and input pulse energy. This work extends the theoretical study of MPCs operating in the EFCR to bulk materials, showing the possibility of obtaining clean ultrashort pulses with minimal secondary structure close to the single-cycle regime in a robust all-bulk configuration.

2 Results and discussion

2.1 Conditions

There are several conditions that have to be fulfilled in order to be in the EFCR that will help us to define a good MPC setup. First, both the self-phase modulation (SPM) and the material dispersion must be relevant effects during the propagation of the pulse. One way to ensure this condition is to maintain the interaction length (L_I) between the nonlinear and the dispersion lengths: ($L_{NL} < L_I < L_D$) [23], where the nonlinear and dispersion lengths are defined as: $L_{NL} = 2/(k_0 n_2 I_0)$ and $L_D = T_0^2/|\beta_2|$ [25]. In these definitions $k_0 = \omega_0/c$ is the wavenumber at the central wavelength of the input pulse, n_2 is the nonlinear refractive index of the nonlinear medium, I_0 is the input peak intensity, T_0 is the temporal duration of the input pulse and β_2 is the group velocity dispersion (GVD) of the nonlinear medium. We have used the full width at half maximum (FWHM) of the intensity temporal profile as T_0 to calculate the dispersion length. Second, to find a robust setup we must avoid the appearance of any self-focusing dynamics, so the width of the bulk material (L) must be much shorter than the collapse length: $L < L_C/10$, where the collapse length, L_C , is defined as in the original Marburger's work ($L_C = 0.367 L_{DF} / \sqrt{[(P_{in}/P_{cr})^{1/2} - 0.852]^2 - 0.0219}$) [26], $L_{DF} = k_0 w_0^2/2$ being the diffraction length, w_0 the spatial width of the input beam, and P_{in} and P_{cr} correspond to the input and critical peak powers, respectively. Last, if we want to achieve ultrashort pulses within the few-cycle regime, as the spectral broadening is limited due to the important stretching of the pulse in the EFCR, we will need to build a cascade setup, based on several MPC stages, paying special attention to the smoothness of the spectral structure of the pulse at the entrance of each stage to avoid any coupling between the spectral modulations into the propagation dynamics, which would deteriorate the pulse cleanness.

2.2 First stage design and results

In order to study how to achieve clean ultrashort pulses in bulk MPC setups, we have simulated the compression process solving the nonlinear propagation equation as described in [23]. We start with a standard 800 nm Gaussian beam with pulse duration $T_0 = 177$ fs (FWHM) ($t_p = 150$ fs) and with 220 μ J of energy. We use two identical fused silica thin plates located on the mirrors of the MPC, while keeping the MPC in vacuum. Regarding the cavity, we use two concave mirrors, both with 7.3 m radius of curvature, separated 40 cm, so that the linear fundamental mode has a waist of 500 μ m and is located at the center of the cavity. We assume a perfect coupling of the beam into the fundamental mode of the cavity. To decide the width of the fused silica plates (L) and the number of round trips (N_{RT}), we have to consider the conditions to be in the desired robust EFCR. The input peak intensity at the plates is 2.86×10^{11} W/cm² with a corresponding peak power of 1.7 GW, much greater than the critical power of fused silica at 800 nm. Taking into account the input peak intensity and the temporal duration of the pulse, and that $\beta_2 = 36.163$ fs²/mm (obtained from the Sellmeier's formula [27]) and $n_2 = 2.22 \times 10^{-20}$ m²/W for fused silica at 800 nm [28], we obtain the following values for the nonlinear, dispersion and collapse lengths: $L_{NL} = 0.4$ cm, $L_D = 27.7$ cm and $L_C = 2.8$ cm. As the beam goes through the fused silica plates four times per round trip, the interaction length for our configuration can be written in terms of the plate width and the number of round trips as $L_I = 4N_{RT}L$, so that the two first conditions are described by: $L_{NL}/(4N_{RT}) < L < L_D/(4N_{RT})$ and $L < L_C/10$. The lilac filled area of Fig. 1(a) shows the possible widths of the fused silica plates to fulfill these two conditions, depending on the number of round trips of the design. For this first stage, we have chosen a standard number of round trips, 40, so according to the limitations of the dispersion, nonlinear, and collapse lengths, a pair of fused silica plates of 500 μ m perfectly fulfill all the conditions. We have represented our choice with an asterisk in Fig. 1(a). A similar procedure will be performed for the next stages, but using the new input peak intensity achieved after the compression of the pulse obtained in the previous stage. Intuitively, the following MPC stages will start with shorter and more intense pulses, so they will have to use less material and/or less round trips to assure keeping the compression process in the EFCR. In our particular case of a cascade scheme with three stages, the last one becomes a single pass through a single fused silica plate instead of a MPC setup (see Fig. 1(b) for the total nonlinear material width for the three stages proposed in this work). This is what we have called an all-bulk hybrid cascade MPC scheme, as not all the stages of the cascade scheme are MPC setups.

With this configuration for the first stage (two 500 μ m fused silica glass plates located on the mirrors and 40 round trips) we obtain a clean short Transform Limited pulse (TL) at the end of the

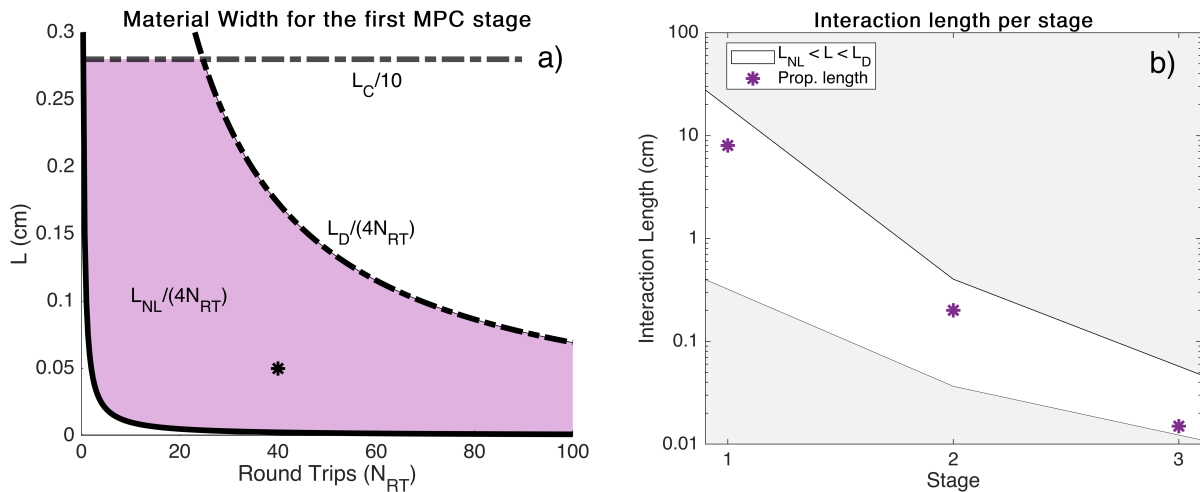


Figure 1: Width of the fused silica plates as a function of the number of round trips (left panel) for the first stage. The lilac region represents the (L, N_{RT}) region for which the propagation is in the EFCR. The right panel shows the interaction length in each stage to operate in the EFCR.

first stage, with a compression factor above 8 (from 177 fs FWHM to 20.7 fs), as shown in the inset box of Fig. 2(a). In Fig. 2(c) we show the spectral evolution that makes this possible. During the first round trips, the pulse undergoes significant spectral broadening due to the self-phase modulation induced by the high peak intensity present during this part of the propagation. The created spectrum is highly modulated because the dispersion accumulated is not enough yet to rearrange it, as can be seen in the purple curve in Fig. 2(b) which shows the on-axis spectral intensity obtained after 15 round trips. From the temporal point of view, the pulse stretches in accordance with the positive linear and nonlinear GVD and the nonlinear spatial readjustments. Obviously, there is an important decrease of the duration of the TL pulse (see Fig. 2(d)) although, during this first part of the propagation, it still shows considerable high side structures linked to the noticeable modulations of the corresponding spectrum. A quantifiable parameter to measure how well the spectral broadening behaves, in terms of pulse quality, is the spectral cleanness, closely related to the TL pulse structure, which gives us an idea about how well filled the spectrum is. We define the spectral cleanness (SC) as the visibility of the spectral modulations, $SC = 2I_m / (I_M + I_m)$, where I_M and I_m are the highest and lowest spatially integrated spectral intensity values inside the spectral width [23]. In general, the higher the SC, the lower the side lobes of the TL pulse structure. In our case we begin with a perfect Gaussian pulse ($SC=1$, without side lobes) and during this first part of the propagation the cleanness decreases in accordance to the modulated spectral broadening process (see Fig. 2(d)).

After approximately 25 round trips, the spectral broadening stops increasing but the nonlinearity, together with the linear dispersion, begins to effectively fill the spectral modulations and broaden the spectral tails, two clear signals of the EFCR in which the propagation is taking place. We can also observe in Fig. 2(d) that the spectral cleanness keeps increasing, reaching values close to 1 again, which means that the side lobes of the TL pulse are disappearing. At the end, after 40 round trips, the maximum intensity of the first side lobe is below 0.3% of the peak intensity, as shown in Fig. 2(a). To finish this discussion on the results for the first stage, we have examined if it could be beneficial to maintain the propagation of the beam a few more round trips in the cell and, furthermore, the feasibility of compensating the spectral phase acquired during the nonlinear propagation. We have checked that if we let the pulse propagate during a few more round trips, there is little impact in spectral broadening, the duration of the TL pulse or the final pulse cleanness. The main reason for the lack of significant improvement is the long temporal duration of the pulse after the first 40 round trips that inhibits any further nonlinear dynamics.

Regarding the spectral phase of the pulse, we have looked into the evolution of the first dispersion orders during the propagation: group delay dispersion (GDD), third order dispersion (TOD), fourth order dispersion (FOD), fifth order dispersion (FiOD) and sixth order dispersion (SOD). These values are calculated by finding the best fit between the temporal profile of the pulse at each propagation distance and the pulse obtained when adding a particular expansion of the spectral phase (up to sixth order) to the modulus of the corresponding spectrum. In Fig. 3, we show the evolution of the on-axis spectral width, $\Delta\omega$ (a), and the different contributions of the spectral phase over the propagation, i.e. $GDD(\Delta\omega)^2/2!$, $TOD(\Delta\omega)^3/3!$, $FOD(\Delta\omega)^4/4!$, etcetera, (b), which gives us an idea about which terms contribute more. We can see that the main contribution comes from the quadratic term, the GDD, so compensating for this term will be enough to retrieve a short pulse. Nevertheless, the fourth order is not negligible and must also be taken into consideration if we want to retrieve clean pulses. On the other hand, odd dispersion terms do not seem to play a relevant role in the pulse dispersion. Here the most dominant terms are the GDD and FOD.

Finally, as we have a relatively complex spatio-spectral nonlinear evolution of the beam, we should verify that we are always below the damage threshold of the plates. For the case of a fused silica plate,

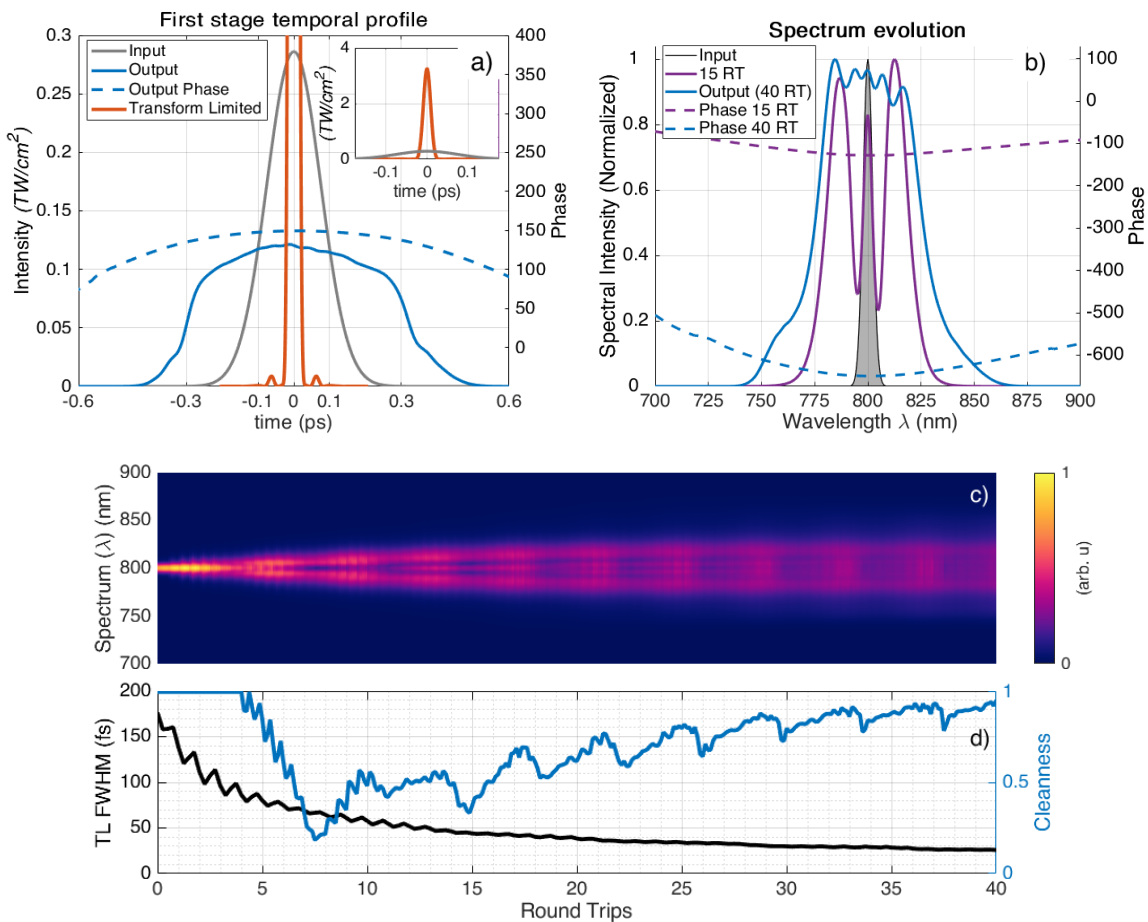


Figure 2: (a) Temporal on-axis intensity distribution of the input (gray), output (blue) and the corresponding Transform Limited (TL) of the output (orange) beam. The dashed-blue line shows the on-axis temporal phase of the output beam. The inset depicts the input and the TL output pulse beams in a different intensity scale to show the full height of the latter. (b) On-axis spectral distribution during propagation at the starting point (gray), after 15 (purple) and 40 (blue) round trips. The dashed-purple and dashed-blue lines show the on-axis spectral phase of the beam after 15 and 40 round trips, respectively. On-axis spectral intensity (c), and cleanliness (blue) and on-axis TL pulse duration (black) (d) during the propagation in the MPC.

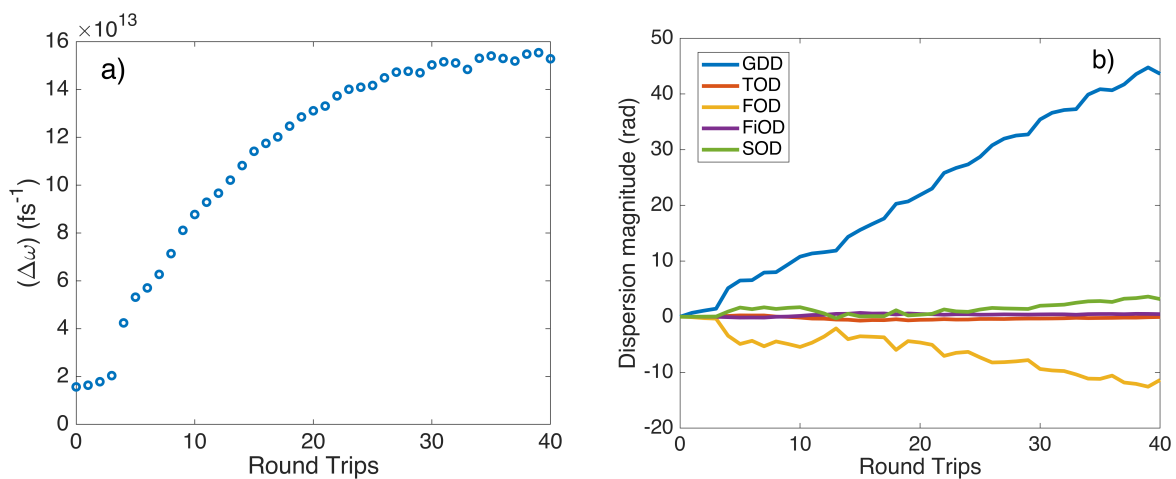


Figure 3: Evolution of the on-axis spectral width ($\Delta\omega$) (a) and the different contributions of the spectral phase up to sixth order (b) during the propagation. The phase contributions are presented as $\text{GDD}(\Delta\omega)^2/2!$, the quadratic contribution, $\text{TOD}(\Delta\omega)^3/3!$ the cubic, etcetera.

the damage threshold of a 150 fs laser pulse at 800 nm is around 3 J/cm^2 [29], and we have checked that we are always well below that value, reaching a maximum fluence value of 0.11 (0.15 and 0.09) J/cm^2 at the first (second and third) stage.

2.3 Second stage and results

In order to further compress our pulse into a shorter one, we need another compression stage. We propose to use the compressed output pulse from the previous stage as the input pulse for a second MPC stage. This new stage will have the same parameters as the first one, except for the fused silica plate thickness and the number of round trips, which will be recalculated to ensure that the propagation remains in the EFCR. To do so, we need to know the peak intensity and the temporal FWHM duration of the input beam, which depends on the compression of the output pulse after the first stage. In Table 1 we discuss two different situations based on using the Transform Limited pulse (TL) obtained from the first stage (top row), i.e. a perfect compression, or the pulse obtained after compensating up to fourth order (GDD, TOD and FOD) (bottom row). With these values we choose the width of the fused silica plates and the number of round trips so that $L_{NL}/(4N_{RT}) < L < L_D/(4N_{RT})$ and $L < L_C/10$ are fulfilled. As expected, the width of the plates and/or the number of round trips have to decrease notably. Our choice is to use two plates of $100 \mu\text{m}$ width and 5 round trips, decreasing the L_I from 8 cm in the first stage to 0.2 cm in the second, as shown in Fig. 1(b).

	I (W/cm^2)	FWHM (fs)	L_D (cm)	L_{NL} (cm)	L_C (cm)
Fourier Limit	3.25×10^{12}	20.7	0.38	0.04	0.91
Up to FOD	3.12×10^{12}	21.3	0.40	0.04	0.93

Table 1: Input pulse peak intensity and pulse duration at the entrance of the second stage after compensating the phase of the output pulse at the first stage in two different ways, and the corresponding dispersion, nonlinear and collapse lengths in each case.

In Fig. 4, we show the on-axis intensity and phase of the output spectrum after propagating 5 round trips in the second stage using the TL pulse (a) or the pulse after compensating the first three dispersion terms (b) as the input pulse. The phase added to the pulse in the non-perfect compression case contained -3515 fs^2 of GDD, -800 fs^3 of TOD and $238.6 \cdot 10^3 \text{ fs}^4$ of FOD, which can be imprinted with custom compressors such as GRISM based systems [30], for example. The propagation of any of these two pulses induces dynamics akin to those observed in the first stage, allowing for further compression of the pulse. For the TL pulse case, Fig. 4(a), the spectral broadening is significant, with a relatively clean spectral phase and with a relatively high spectral cleanliness ($\text{SC}=0.64$), as desired. This spectrum is compatible with a TL pulse of 6.73 fs FWHM duration and in which the maximum intensity of the first side lobe reaches 0.06% of the peak intensity. For the more realistic case of the pulse obtained after compensating the output pulse of the first stage up to the FOD, Fig. 4(b), the spectral broadening, phase and cleanliness deteriorate as the input pulse is less intense and not as clean as in the ideal TL case. In this case, the spectrum ($\text{SC}=0.54$) is compatible with a TL pulse of 7.15 fs FWHM duration, and in which the maximum intensity of the first side lobe reaches 0.24% of the peak intensity.

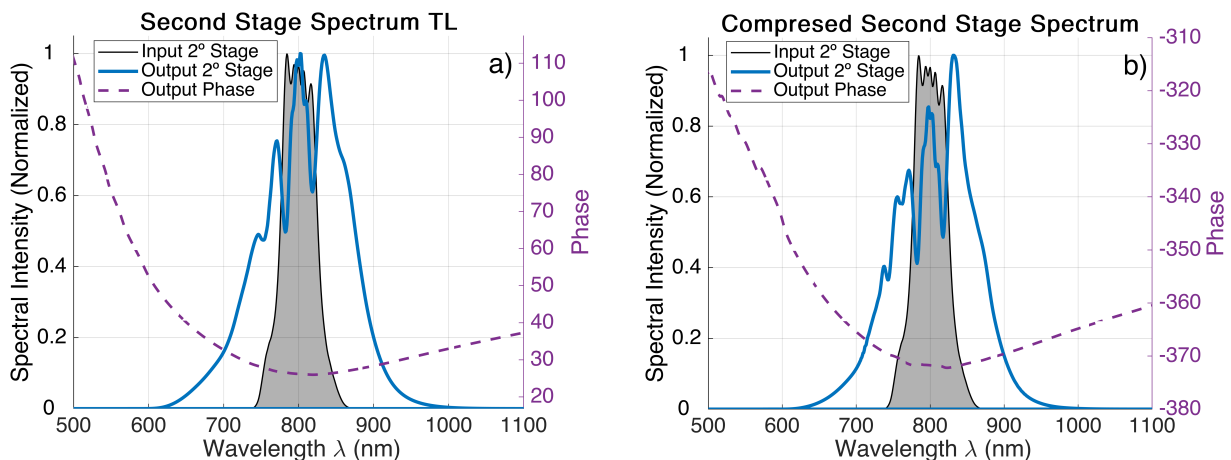


Figure 4: On-axis output spectra and phase obtained from the second stage when introducing (a) the TL pulse or (b) the pulse after compensating for GDD, TOD and FOD.

2.4 Third (final) stage and results

If we want to have a pulse in the few-cycle regime with this technique we have to repeat the process a third time. The procedure, once more, starts by compensating the output pulse obtained from the second stage and use it as the input pulse for the next stage. With the new pulse we have to

design the new stage to keep in the EFCR. Taking as the input pulse for this last stage the TL pulse of the spectrum shown in Fig. 4(a) we obtain an input pulse with 6.73 fs FWHM duration and a peak intensity of 1.08×10^{13} W/cm². We will call this the TL path, as we always use the TL pulse of the previous stage as the input pulse of the next one. In this case, the lengths that help us to design each stage take the following values: $L_D = 0.403$ mm, $L_{NL} = 0.106$ mm and $L_C = 3.73$ mm. Again, the width of the plates and/or the number of round trips have to be decreased compared to the previous stage. With these typical lengths, it has not much sense to use a third MPC and it is preferable to use a single-pass thin-plate configuration. In particular, we propose to take the beam from the compressor after the second stage and let it first propagate through vacuum as typically done in the standard thin-plate configuration [31, 32]. The beam size of the TL pulse after 40 cm of free vacuum propagation grows and the peak intensity decreases to 9.60×10^{12} W/cm², so $L_{NL} = 0.121$ mm. Therefore, we have to find the width of the thin-plate that fulfills that $L_{NL} < L < L_D$ and $L < L_C/10$, where we have taken into account that now the interaction length coincides with the length of the plate, $L_I = L$. Our choice, then, is to use a 150 μ m fused silica thin-plate which keeps the nonlinear propagation in the EFCR, as shown in Fig. 1(b). The on-axis spectrum obtained after the thin-plate for the ideal TL path is shown in Fig. 5(a), which corresponds to a TL pulse of 3.88 fs FWHM duration and in which the maximum intensity of the first side lobe reaches 0.03% of the peak intensity. If we calculate a more realistic pulse (Fig. 5(b)) in which we compensate the three more relevant dispersion terms (GDD, TOD and FOD), we achieve a pulse with 3.93 fs FWHM duration and in which the maximum intensity of the first side lobe reaches 0.15% of the peak intensity. Either of the two results are few-cycle clean pulses as we desire.

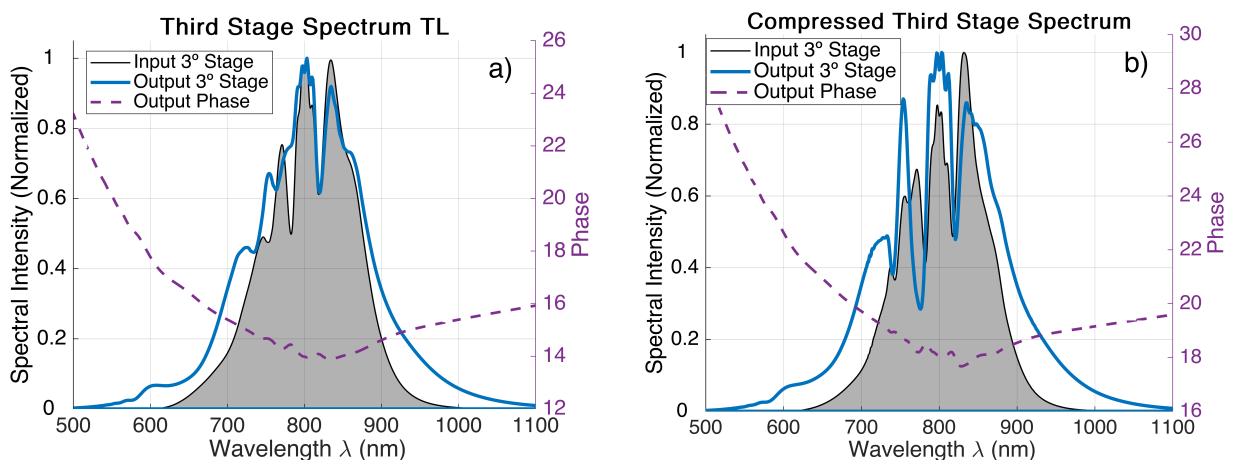


Figure 5: On-axis output spectra and phase obtained from the third stage when following (a) the TL path or (b) a more realistic situation in which the output pulses of all stages are compensated for GDD, TOD and FOD.

3 Conclusion

In this work, we have presented a comprehensive study of pulse compression using a three-stage all-bulk hybrid multipass cell (MPC) scheme, demonstrating its ability to achieve ultrashort and high-quality optical pulses. Operating in the enhanced frequency chirp regime (EFCR), we have compressed pulses from 177 fs FWHM to pulses with 3.88 fs transform limited duration and side lobes whose maximum intensity value is below 0.2% of the main peak intensity. The optimal conditions for EFCR propagation have been carefully established, ensuring controlled and efficient spectral broadening and clean temporal profiles. The first two stages use bulk MPCs to achieve smooth spectral broadening, while a third stage uses a thin plate to extend the spectral bandwidth while preserving the pulse temporal quality. After each stage, the pulse phase is compensated. This robust, all-bulk approach highlights the potential of MPC designs for generating clean, few-cycle pulses, with applications in attosecond science and ultrafast optics.

References

1. Krausz, F. & Ivanov, M. Attosecond physics. *Rev. Mod. Phys.* **81**, 163–234 (2009).
2. Gamaly, E. G. The physics of ultra-short laser interaction with solids at non-relativistic intensities. *Physics Reports* **508**, 91–243 (2011).
3. *Ultrashort Pulse Laser Technology: Laser Sources and Applications* en (eds Nolte, S., Schrepel, F. & Dausinger, F.) (2024) (Springer International Publishing, Cham, 2016).
4. Nagy, T., Simon, P. & Veisz, L. High-energy few-cycle pulses: post-compression techniques. en. *Advances in Physics: X* **6**, 1845795. ISSN: 2374-6149. (2022) (Jan. 2021).

5. Khazanov, E. Post-compression of femtosecond laser pulses using self-phase modulation: from kilowatts to petawatts in 40 years. en. *Quantum Electronics* **52**, 208–226. ISSN: 1063-7818, 1468-4799. (2022) (Mar. 2022).
6. Schulte, J., Sartorius, T., Weitenberg, J., Vernaleken, A. & Russbuedt, P. Nonlinear pulse compression in a multi-pass cell. en. *Optics Letters* **41**, 4511. ISSN: 0146-9592, 1539-4794. (2022) (Oct. 2016).
7. Hanna, M. *et al.* Nonlinear Optics in Multipass Cells. en. *Laser & Photonics Reviews* **15**, 2100220. ISSN: 1863-8880, 1863-8899. (2022) (Dec. 2021).
8. Viotti, A.-L. *et al.* Multi-pass cells for post-compression of ultrashort laser pulses. en. *Optica* **9**, 197. ISSN: 2334-2536. (2022) (Feb. 2022).
9. Herriott, D., Kogelnik, H. & Kompfner, R. Off-Axis Paths in Spherical Mirror Interferometers. en. *Applied Optics* **3**, 523. ISSN: 0003-6935, 1539-4522. (2022) (Apr. 1964).
10. Jargot, G. *et al.* Self-compression in a multipass cell. EN. *Optics Letters* **43**, 5643–5646. ISSN: 1539-4794. (2022) (Nov. 2018).
11. Gröbmeyer, S. *et al.* Self-compression at 1 μm wavelength in all-bulk multi-pass geometry. en. *Applied Physics B* **126**, 159. ISSN: 0946-2171, 1432-0649. (2023) (Oct. 2020).
12. Carlson, D. *et al.* Nonlinear post-compression in multi-pass cells in the mid-IR region using bulk materials. EN. *Optics Letters* **47**, 5289–5292. ISSN: 1539-4794. (2022) (Oct. 2022).
13. Liu, Y. *et al.* Few-cycle 12.5-GW pulses generated via efficient all-solid-state post-compression from an ytterbium laser. en. *Optics Letters* **49**, 6992. ISSN: 0146-9592, 1539-4794. (2024) (Dec. 2024).
14. Seidel, M. *et al.* Factor 30 Pulse Compression by Hybrid Multipass Multiplate Spectral Broadening. en. *Ultrafast Science* **2022**, 2022/9754919. ISSN: 2765-8791. (2023) (Jan. 2022).
15. Escoto, E. *et al.* Temporal quality of post-compressed pulses at large compression factors. EN. *JOSA B* **39**, 1694–1702. ISSN: 1520-8540. (2022) (July 2022).
16. Pajer, V. & Kalashnikov, M. High temporal contrast ultrashort pulses generated by nonlinear ellipse rotation in multipass cells. en. *Laser Physics Letters* **18**, 065401. ISSN: 1612-2011, 1612-202X. (2024) (June 2021).
17. Song, J., Shen, L., Sun, J., Peng, Y. & Leng, Y. Temporal contrast enhancement via nonlinear elliptical polarization rotation in a solid thin plate. en. *Optics Express* **30**, 26297. ISSN: 1094-4087. (2024) (July 2022).
18. Kaur, J. *et al.* Simultaneous nonlinear spectral broadening and temporal contrast enhancement of ultrashort pulses in a multi-pass cell. en. *Journal of Physics: Photonics* **6**, 015001. ISSN: 2515-7647. (2024) (Jan. 2024).
19. Escoto, E. *et al.* Improved temporal characteristics for post-compressed pulses via application-tailored nonlinear polarization ellipse rotation. en. *Optics Letters* **49**, 6841. ISSN: 0146-9592, 1539-4794. (2024) (Dec. 2024).
20. Grischkowsky, D. & Balant, A. C. Optical pulse compression based on enhanced frequency chirping. *Applied Physics Letters* **41**, 1–3 (1982).
21. Tomlinson, W. J., Stolen, R. H. & Shank, C. V. Compression of optical pulses chirped by self-phase modulation in fibers. EN. *JOSA B* **1**, 139–149. ISSN: 1520-8540. (2022) (Apr. 1984).
22. Benner, M., Karst, M., Amaya Mendez, C., Stark, H. & Limpert, J. Concept of enhanced frequency chirping for multi-pass cells to improve the pulse contrast. en. *Journal of the Optical Society of America B* **40**, 301. ISSN: 0740-3224, 1520-8540. (2023) (Feb. 2023).
23. Staels, V. W. S. *et al.* Numerical investigation of gas-filled multipass cells in the enhanced dispersion regime for clean spectral broadening and pulse compression. EN. *Optics Express* **31**, 18898–18906. ISSN: 1094-4087. (2023) (June 2023).
24. Karst, M., Benner, M., Gierschke, P., Stark, H. & Limpert, J. Dispersion engineering in nonlinear multipass cells for high-quality pulse compression. en. *Optics Letters* **48**, 5899. ISSN: 0146-9592, 1539-4794. (2023) (Nov. 2023).
25. Agrawal, G. P. *Nonlinear Fiber Optics* (Academic Press, 2013).
26. Marburger, J. Self-focusing: Theory. en. *Progress in Quantum Electronics* **4**, 35–110. ISSN: 00796727. (2024) (Apr. 1975).
27. Malitson, I. H. Interspecimen Comparison of the Refractive Index of Fused Silica^{*,†}. EN. *JOSA* **55**, 1205–1209. (2022) (Oct. 1965).
28. Schiek, R. Nonlinear refractive index in silica glass. en. *Optical Materials Express* **13**, 1727. ISSN: 2159-3930. (2023) (June 2023).

29. Chimier, B. *et al.* Damage and ablation thresholds of fused-silica in femtosecond regime. en. *Physical Review B* **84**, 094104. ISSN: 1098-0121, 1550-235X. (2025) (Sept. 2011).
30. Dou, T. H. *et al.* Dispersion control with reflection gratings of an ultra-broadband spectrum approaching a full octave. en. *Optics Express* **18**, 27900. ISSN: 1094-4087. (2025) (Dec. 2010).
31. Zhu, B. *et al.* Spatially homogeneous few-cycle compression of Yb lasers via all-solid-state free-space soliton management. EN. *Optics Express* **30**, 2918–2932. ISSN: 1094-4087. (2022) (Jan. 2022).
32. Tsai, M.-S. *et al.* Nonlinear compression toward high-energy single-cycle pulses by cascaded focus and compression. en. *Science Advances* **8**, eabo1945. ISSN: 2375-2548. (2025) (Aug. 2022).